Scientific Research Publishing

Energy and Power Engineering, 2023, 15, 151-179
https://www.scirp.org/journal/epe
ISSN Online: 1947-3818
ISSN Print: 1949-243X

Battery-Free Power Supply for Wireless Sensor Combining Photovoltaic Cells and Supercapacitors

Vincent Boitier[1], Bruno Estibals[1], Florian Huet[2], Lionel Seguier[1]

[1]LAAS-CNRS, Université de Toulouse, Toulouse, France
[2]LISPEN, Arts et Metiers Institute of Technology, HESAM Université, Aix-en-Provence, France
Email: vincent.boitier@laas.fr

How to cite this paper: Boitier, V., Estibals, B., Huet, F. and Seguier, L. (2023) Battery-Free Power Supply for Wireless Sensor Combining Photovoltaic Cells and Supercapacitors. *Energy and Power Engineering*, **15**, 151-179.
https://doi.org/10.4236/epe.2023.153007

Received: January 30, 2023
Accepted: March 17, 2023
Published: March 20, 2023

Abstract

This article exhibits the sizing, modelling, and characterization of a power supply (output 3.3 V, 200 mA max, 11 days full autonomy) dedicated to powering a wireless sensor node without a battery but usable as simply as with a battery. This system is modular for various light levels (indoor and outdoor). It is easily integrable into a sensor node, using only commercial circuits. The choices of the photovoltaic surface (amorphous silicon, η 5%, 35 cm^2) and of the supercapacitors value (2x 25F, 2.7 V) are explained for permanent operation, considering the solar potential and the consumption. An original part of the paper is devoted to the issue of the startup, in which we demonstrate that after a particular preload, once installed, the device can start on request at the desired time (within 15 days) using as a trigger any light source, such as the LED of a mobile phone.

Keywords

Photovoltaic, Energy Harvesting, Free Battery System, Energy Management, Supercapacitor

1. Introduction

1.1. State of the Art

The deployment of Internet of Things (IoT) in the industrial, agriculture [1], transport, and health sectors [2] has been soaring over the past few years. The use of Wireless Sensors Networks (WSNs) has become a solution to achieve the objectives of performance improvement, mainly due to its wide range of utility in remote monitoring.

WSNs face the challenge of having a limited energy source available onboard, where packet transmission and sensing functions are the most power-consuming factors. To overcome energy depletion, it is important to study the energy management issue in WSNs.

Over the last decade, the performances of low-power electronics have increased considerably. Consequently, low-power sensors are now available at low prices and, when combined with sensors algorithms that adapt the tasks (measurement, transmission), WSN consumption has decreased. More recently, current radio protocols (BLE, NB-IoT, Lora) offer energy-saving solutions, even on long distances, with very good performance levels [3].

1.1.1. Working Life for Battery Power Device

In many cases, the sensors are simply powered by rechargeable or non-rechargeable batteries. For example, Movesolutions society uses for a tiltmeter a 100 g Lithium battery type D of 19 Ah 3.6 V. This wireless sensor is waterproof IP67 and it operates in the range −40˚C, +85˚C. The device transmits in Lora the measured angle at regular time intervals. It is fully wireless; its battery offers eight years of autonomy [4]. Similarly, the BT510 Bluetooth 5 sensor platform of Laird is powered with a replaceable coin cell battery (CR2477, 3 V, 1000 mAh) and can operate for years in the field. The BT610 is a little bigger and powered with a primary Lithium battery type AA 3.6 V, 2400 mAh. For this product, Laird offers to use a tool to estimate battery life (typically 5 years) [5].

For indoor Lorawan wireless sensors, the company Elsys also shares a similar tool [6]. On their ERS CO_2 device, the estimated battery life is up to 10 years, but this depends on the sample interval, transmit interval, data rate, and environmental factors. It is powered by two 3.6 V AA lithium batteries.

Similarly, Milesight-IoT Company has announced an autonomy of between 5 and 10 years for its indoor temperature and humidity sensors [7] and Wika has announced the same for its battery-powered wireless instruments for pressure, temperature, level, and force [8].

Nevertheless, energy autonomy remains a key point in the sizing of a sensor node. Indeed, the lifetime of the battery that powers a sensor node remains a major bottleneck. In best cases, 5 or 10 years are expected. “But some batteries run out of power earlier than others, some of them are difficult to reach” [9]. Therefore, battery replacement has become a major drawback for industries that deploy many sensors. In this context, energy harvesting becomes an attractive option. In fact, routine maintenance and material costs are canceled as sensor nodes become maintenance-free with energy harvesting solutions.

1.1.2. Harvesting Solution

Energy harvesting is based on a process by which energy is derived from external sources, such as solar power [10], thermal energy, wind energy, salinity gradients, or kinetic energy (also known as ambient energy), and captured, and stored for small, wireless autonomous devices. The storage block is mandatory

to provide the output power despite the intermittency and possible variations of the ambient energy.

Today, around a dozen of commercial integrated electronic circuits are sold as "energy harvesters" in the WSN power range, for example, SPV1050 from STMicroelectronics (chosen in our study and used in [11] [12]), ADP5090, LTC3105, TLC3108 from Analog Devices, BQ25504, BQ25570 from Texas Instruments used in [11], ECT310 from EnOcean, EM8502 from EM microelectronics, used in [12], Energy Harvesting Boost Converter from Matrix Industries, EH4205 from Advanced Linear Devices and AEM10941 from e-peas, used in [11].

Driving by the environment close to the node sensor, the harvested energy is extracted using an adapted transducer (photovoltaic cells, thermos-electro-generator, piezoelectric beam, rectenna antenna…).

Driving close to the node sensor, the harvested energy is extracted using an adapted transducer. In the following, this article will focus on indoor or outdoor light harvesting, although the ideas developed could be directly extended to systems powered by a thermoelectrogenerator using the same electronic circuits.

Sensors powered with energy harvesting have a long operating time, minimum 15 years. More, compared to a sensor node powered solely by a primary battery, the device which combines a rechargeable battery and an energy harvesting system [13] [14] may increase the measurement rate if the amount of harvested energy is favorable.

To minimize the size of the rechargeable battery, the association of battery and supercapacitor [15] [16] is a solution as short current peaks generated during radio transmissions are not available from any regular 3V Lithium battery type.

1.1.3. Battery Free System

The next step consists of eliminating the battery and using a battery-free energy harvesting system. Indeed, a supercapacitor offers a very interesting lifetime (more than 300,000 cycles vs 500 for a rechargeable battery), often a larger range of temperature (typically [−40, 85]˚C for a PC10 supercapacitor vs [−20, 45]˚C for a LIR 2450-coin cell battery), and it can accept high peak currents. Unfortunately, the energy density of a supercapacitor is lower than that of a battery and the leakage current could be not negligible for a supercapacitor. These drawbacks are cleared when the daily average ambient power is sufficient to avoid long periods of complete autonomy of the node.

Despite these drawbacks, industrial sensors offer the user the option of a rechargeable battery or substituting it with a supercapacitor storage element [17]. Long term tests (more than 2 years) showed the maturity of free battery solution in IoT for smart agriculture [18]. For example, commercial battery-free products such as sealed (IP65) vibration sensors [19] [20] or indoor environment sensors are now available, but this is still a niche market. So, compared to a primary battery solution, and despite its initial higher cost, a battery-free, self-powered solution appears to be an ideal choice for remote monitoring sensors in hard-to-access

locations and sites or in high-temperature environment. It is important to notice that like batteries, waste supercapacitors should be recycled according to EU directive 2002/96/EC on waste electric and electronic equipment.

A battery-free solution must overcome some obstacles.

A first important point is the sizing of the different components. It depends on the available ambient energy (light potential in the case of a photovoltaic solution), the consumption and must be carefully taken into account the different losses [21] [22] [23]. It must be realized without oversizing the elements for a massive deployment at a good price and volume.

The second point deals with the issue of the startup. Indeed, if the startup of a sensor node powered by a battery is immediate as soon as the battery is connected, this is not the case when the storage is performed with initially empty supercapacitors. Industrialists do not discuss the startup of battery-free sensor nodes, and this is generally the same in research papers [24] [25] [26].

However, it is a real problem in complex industrial environments or in case of long-range transmission. Some articles present the restart after a phase without energy recovery [27], and to avoid the cold start, a preload is sometimes used during laboratory tests [28]. But very few papers address the cold start issue [29] [30].

With initially empty supercapacitors, thanks to the harvested power, the supercapacitors voltage increases but slowly (low efficiency phase). It is necessary to wait until the voltage at the terminals of the supercapacitors reaches a targeted level, before properly supplying the load.

This cold-start phase is often too long and does not allow an immediate signal from the sensor during its positioning on site. Of course, it is necessary to validate the radio communication of the sensor node. This means that the installer may have to wait for hours before the effective startup of the device, especially in indoors applications with low harvested power.

1.2. Objectives and Contents of the Paper

1.2.1. Objectives

This article uses a classical solution using supercapacitors as storage stage and photovoltaics for energy harvesting. The objectives of the paper are firstly to propose a rigorous sizing methodology, and secondly to explain an interesting solution to avoid the drawback of a long startup and to facilitate the commissioning of the device.

The main new feature is the explanation of the method for preparing the initial startup. The original solution consists of both a preload with required conditions that minimizes leakages in supercapacitors, and after an external activation of the sensor node. Activation is carried out at the desired time without opening the enclosure, allowing the system to be completely sealed. In fact, once the solar cells' dark protection has been removed, activation is instantaneous when the solar cells are exposed to even a brief burst of natural light or the flash of a smartphone.

1.2.2. Contents

This paper presents a 3.3 V 200 mA power supply dedicated to power a wireless sensor node without a battery, but as easily as with a battery. This system, modular for different light levels (indoor and outdoor) and easy to integrate in a sensor node, uses only commercial circuits.

The battery-free power supply is build using a small PV panel, a supercapacitor storage and an SPV1050 [31] circuit for energy harvesting and management. The node architecture and its sizing are exhibited in the Section 2 according to the light resource and the sensor consumption. The different parts of the SPV1050 are detailed and characterized.

The use of a photovoltaic harvester with supercapacitors storage is a classic one, well documented in term of its sizing. However, information on the initial start-up issue is very scarce. Section 3 is focused on the start-up issue. The cold start phase is analyzed. A solution to achieve a quick first startup is then detailed, using a specific feature of the SPV1050. The supercapacitors are preloaded without powering the output load and the initial start of all the electronic circuit remains blocked when the solar cells are in darkness. This minimizes the self-discharge of the supercapacitors.

As a result, the supercapacitors discharge very slowly, and the voltage remains favorable for future activation. The result is a potential delay between pre-charging and commissioning of over 3 weeks, which is sufficient for most applications.

Section 4 presents the on-site results of the whole system. Finally, a discussion concludes the article.

2. Structure and Design

2.1. Generator Architecture

In this way, we first use a special circuit, the SPV1050, which recovers electrical energy from a solar panel (5 × 7 cm^2) (**Figure 1**). It includes an MPPT (Maximum Power Point Tracking) function and controls the voltage levels of the storage stage.

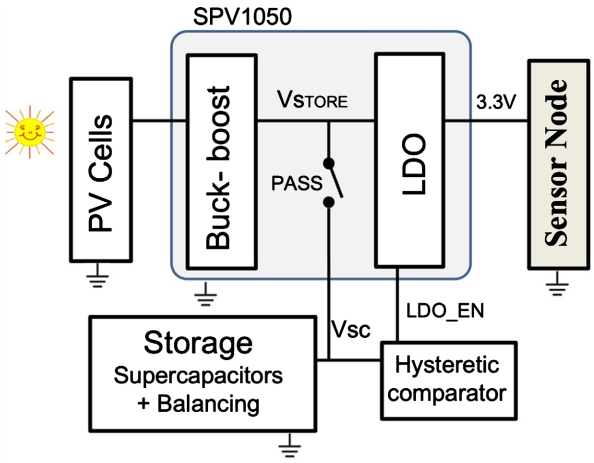

Figure 1. Global structure.

Storage is provided by two supercapacitors associated in series with a voltage balancing circuit (ALD910024). A linear regulator (LDO) integrated into the SPV1050 provides the required voltage level (3.3 V) to power the sensor node. This internal LDO is driven by an external enable signal (LDO_EN), corresponding to the output of a hysteresis comparator connected to the supercapacitor voltage.

2.2. Sensor Node

The wireless sensor node is composed of an ATMEGA328P microcontroller (Arduino) settled in low power with a NRF24L01 radio module, which allows to transmit and receive data on the 2.4 GHz frequency range. When used in open space its range can reach up to 100 meters. This radio module uses the proprietary "ShockBurst" protocol [32]. The Mysensors library [33] allows the NRF24L01 modules to be controlled quickly and easily. To collect and display data from sensors, Jeedom home automation software is used [34]. The flexibility of this software offers the selection of different sensors in a large panel either analog or digital, compatible with the protocols supported by ATMEGA328P. Initially, a shield with a temperature sensor based on a DS18b20 is added. The combination of Mysensors and Jeedom makes it easy to set up, store and display measurements.

Typically, a harvesting system is added after the initial design of the sensor node which is powered by a lithium battery. This results in a supply voltage V_{LOAD} = 3.3 V. The current shapes, during initial start-up, sleep, measurement, and transmission phases are shown in **Figure 2**. Measurements are performed using an Agilent N6705B DC power analyzer and summarized in **Table 1**.

To summarize:

- The initial startup of the sensor node is often highly energy consuming. During this phase, the sensor establishes the connection with the network. The peak current is often reached at the beginning of this phase, especially when the input of the load is capacitive.
- Once the initial startup is completed, the operating cycle usually breaks down into two modes:
  - sleep mode with a very low power consumption,
  - active mode during which measurements, data processing and radio transmission are performed. There may be a current peak during this phase depending on the transmission mode.

It is important to carefully analyze the consumption when sizing the storage block. There must be enough energy left in the supercapacitors after the initial start-up. Supercapacitors must be able to provide the required current peaks and the storage must offer the required autonomy.

The initial consumption of the node is noted E_{STARTUP}. The parameters indexed "SLEEP" correspond to the standby phase, the quantities indexed "MEAS" correspond to the measurement and communication phase. The consumption

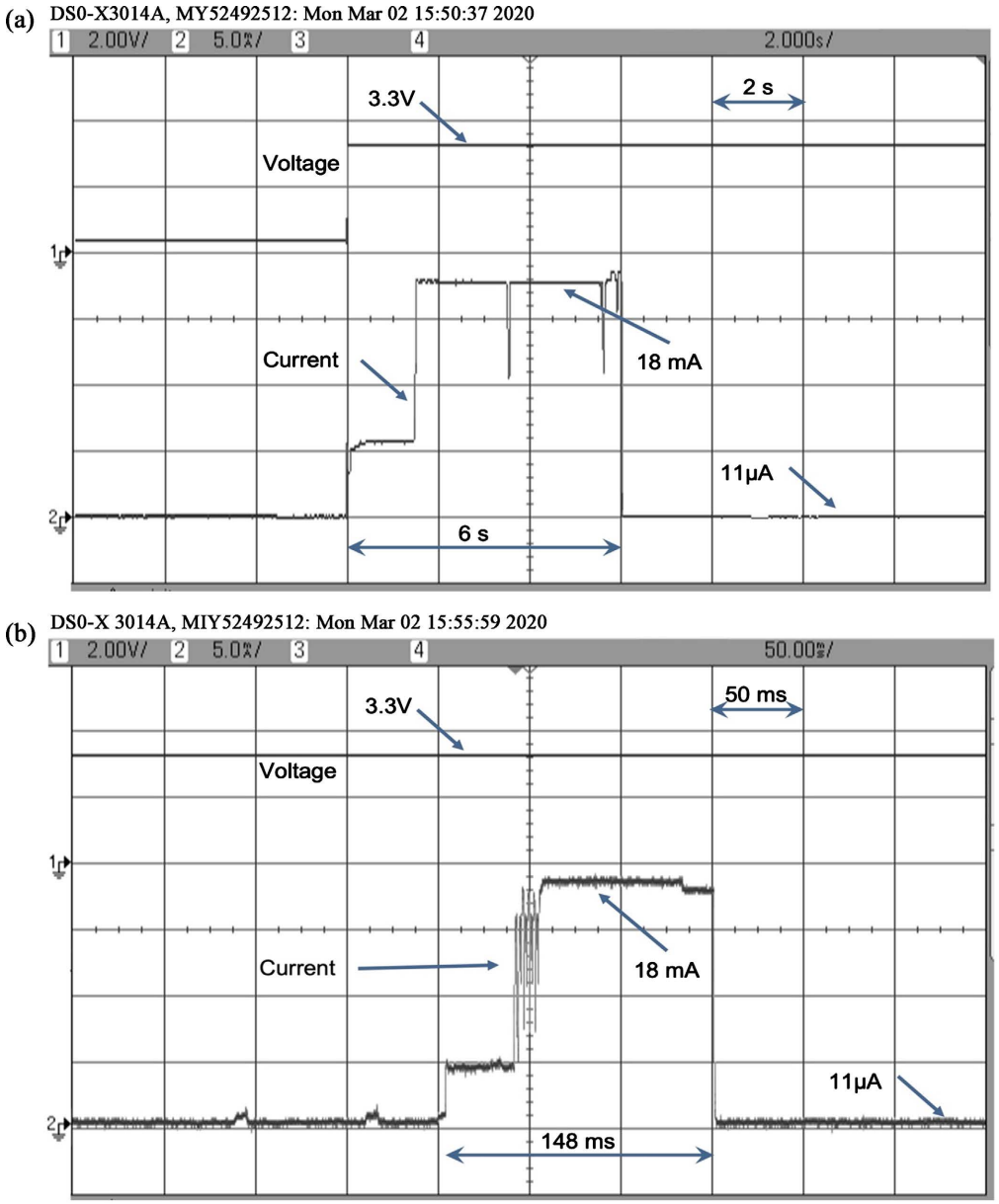

Figure 2. Sensor node: Initial startup (a), measurement and communication phase (b).

Table 1. Sensor node consumption.

Voltage	3.3 V
Startup	
E_STARTUP	272 mJ
T_STARTUP	6.0 s
Measure and Communication	
E_MEAS	6.5 mJ
T_MEAS	148 ms
Sleep mode	
Sleep current	11 µA

per cycle is given by:

$$E_{CYCLE} = E_{SLEEP} + E_{MEAS} = \left(V_{ALIM} \cdot I_{SLEEP}\right) \cdot T_{SLEEP} + E_{MEAS} \quad (1)$$

with:

$$T_{SLEEP} = T_{CYCLE} - T_{MEAS} \approx T_{CYCLE} \quad (2)$$

The average power consumption is easily calculated according to the duration of the measurement cycle. For T_{CYCLE} = 5 min, we find E_{CYCLE} = 17 mJ and $<P_{CYCLE}>$ = 58 µW, and thus with V_{LOAD} = 3.3 V an average current consumed $<I_{LOAD}>$ = 18 µA.

If we decide to reduce the rate of measurement, the average power consumption tends to a limit of 36 µW which corresponds to the power consumed in standby mode (Figure 3).

2.3. Photovoltaic Energy

Usually, sensor node consumption is easily measurable, but it is more difficult to predict the photovoltaic potential before installation on a given site. Nevertheless, an estimate can be obtained using databases and/or direct measurements on site [35] [36].

2.3.1. Light Resource

As far as light energy in indoor condition is characterized by the illumination E (Lux), irradiance G (W/m^2) is used in outdoor condition. Randall [37] proposed a simplified conversion between illumination and irradiance:

$$1\ \text{lux} = 1/120\ \text{W}/\text{m}^2 \quad (3)$$

The literature provides some information to estimate in a first approach the luminous potential according to the location of solar cells. Table 2 shows some typical values.

These values should be considered with caution, especially for indoor

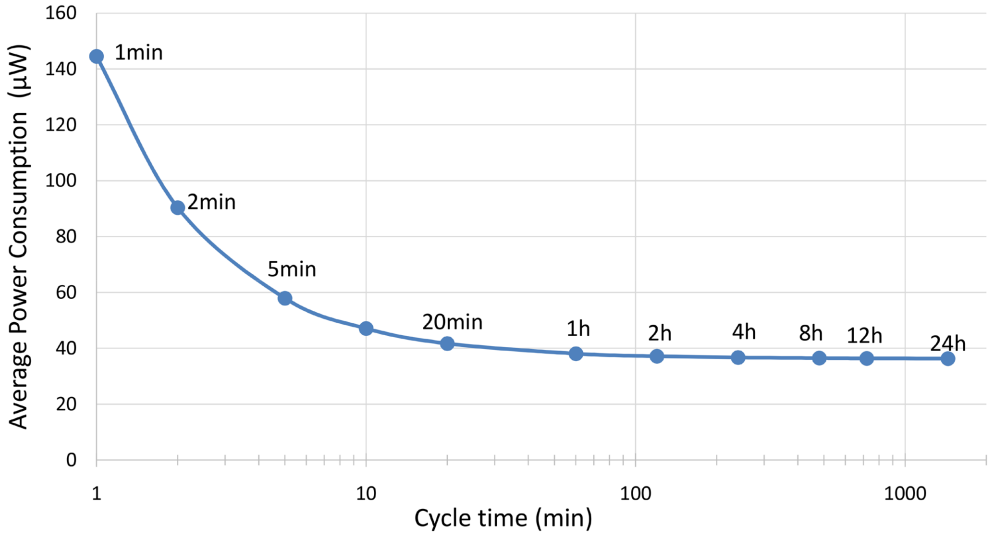

Figure 3. Average power consumed by the sensor node vs measurement rate.

Table 2. Energy available for energy recovery according to [25].

Use case	Indoor				Outdoor	
	Soft lighting	Corridor lighting	work lighting	incandescent bulb	overcast weather	very sunny
E (lux)	80	150	740	1200	3000	100000
G (W/m^2)	0.67	1.3	6.2	10	25	1000

locations [38]. In all cases, we suggest either to maximize the solid angle seen by the solar panel facing windows, or to position the solar panel towards an artificial light source.

For outdoor use, it is also important to assess the importance of masks that block both direct and diffuse radiations. Databases generally provide horizontal daily or hourly irradiations in kWh/m^2. These values should be supplemented by some in situ measurements. For a preliminary study Waltisperger [39] states "the following pessimistic hypothesis (currently used in the industry), […] the photovoltaic collector is positioned in the north and subjected to a rainy winter weather for 6 hours per day, which represents an available solar power density of 20 W/m²". In fact, 20 W/m^2 corresponds to a typical value observed in December by rainy weather in Toulouse, France for a horizontal measurement.

2.3.2. Photovoltaic Panel

1) Required Surface

Simple relations can be used to quickly size the available photovoltaic surface S. By the following, we assume that:

- η_{PV} is the efficiency of the solar cells,
- $\eta_{DC/DC}$ is the efficiency of the SPV1050 Buck/Boost converter,
- η_{LDO} is the efficiency of its internal LDO,
- η_{SC} is the load/discharge efficiency of supercapacitors, assumed to be constant.

If we consider a system placed outdoors which receives an average irradiance G (W/m^2) per day for a duration D (h), the recoverable energy in J/m^2/day is:

$$E_{SUN\_DAY} = G \cdot \left(D \cdot 3600 \right) \tag{4}$$

So, the surface S chosen must verify:

$$\left(E_{SUN\_DAY} \cdot S \right) \cdot \eta_{PV} \cdot \eta_{DC/DC} \cdot \eta_{SC} \cdot \eta_{LDO} \geq E_{CONSO\_DAY} \tag{5}$$

with:

$$E_{CONSO\_DAY} = \left(24 / T_{CYCLE} \right) \cdot E_{CYCLE} \tag{6}$$

For a pre-sizing, we choose:

- η_{PV} = 5% (typical value with amorphous silicon or with crystalline cells at low irradiance),
- $\eta_{DC/DC}$ = 75%, (slightly pessimistic value)
- η_{LDO} = 75%, (depending of the current and the dropout voltage)
- η_{SC} = 80%.

For a system placed outdoors with G = 20 W/m^2 during D = 6 h, Using a measuring rate T_{CYCLE} = 5 min, we find a minimum area S = 5 cm^2. With the same rate, indoor, with an illumination of 300 lux, 7 h per day (office lighting), S = 35 cm^2 is convenient.

2) Photovoltaic Panel Characteristics

Based on SPV1050 voltage range, we selected the Sanyo AM5706CAR amorphous PV module for outdoor and indoor use (Figure 4). Its characteristics for an illumination of 50 klux are:

- S: 5 cm × 7 cm = 35 cm^2,
- V_{OC} = 6 V, I_{SC} = 22.6 mA,

V_{MP} - I_{MP} - P_{MP}: 4.6 V - 19 mA - 88 mW @ 50 klux and 4.6 V - 40 mA - 186 mW @ 100 mW/cm^2 = 1 Sun.

To validate this data, we decided to make our own measurements (Figure 4), which gave:

- V_{OC} = 5.3 V, I_{SC} = 3.1 mA,
- V_{MP} - I_{MP} - P_{MP}: 4.3 V - 2.6 mA - 11.2 mW @ 6000 lux.

In all cases, a photovoltaic efficiency between 5% and 6% for this panel has been found, and the ratio V_{MP}/V_{OC} remains constant. V_{MP}/V_{OC} = 80% ± 4%.

2.4. Energy Storage

Whichever the application aiming a long-time duration storage with many cycles, or high temperature constraints, supercapacitors are becoming more and more interesting [38]. However, the choice of supercapacitors must always be compared with the use of a rechargeable battery.

2.4.1. Supercapacitors Sizing

Simple relationships are generally used to estimate supercapacitors capacity. In a pre-sizing step, certain phenomena can be neglected, such as supercapacitors

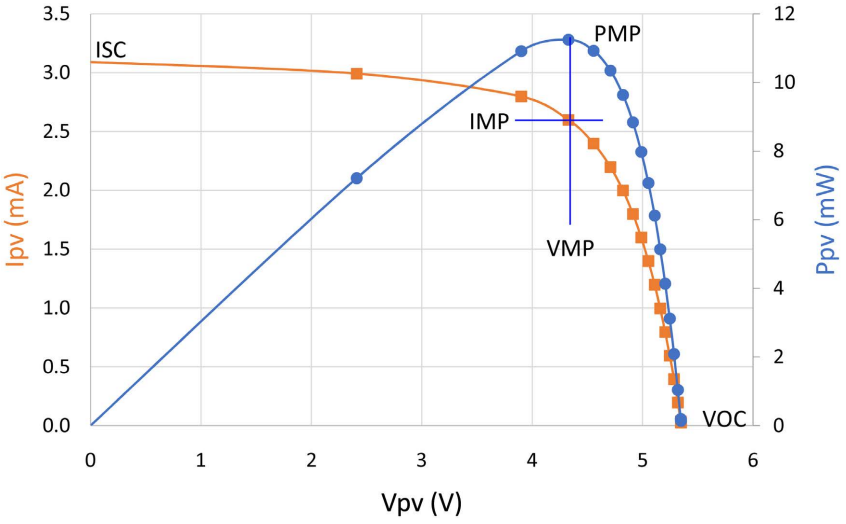

Figure 4. Amorphous PV module ref Sanyo AM-5706 car and characterization of the AM-5706 @6000 lux and 25˚C.

self-discharge, balancing consumption, etc. some of them can be simplified, such as the constant value of the average efficiency, although it depends on the voltage of the supercapacitors and the current flow.

For supercapacitors:

- The equivalent capacity C_{EQ} (F) is calculated according to the desired autonomy -noted Aut (day).
- The supercapacitor voltage evolves over a useful range between $V_{SC\,MAX}$ and $V_{SC\,MIN}$.

In the way to obtain the desired operating time, the energy available in the supercapacitors must be greater than the energy consumed during the phase without any refill. If we neglect losses induced by self-consumption, serial resistance, balancing system, and assuming a constant efficiency for the LDO, we obtain:

$$\frac{1}{2}\cdot C_{EQ}\cdot\left(V_{SC\_MAX}^2 - V_{SC\_MIN}^2\right)\cdot\eta_{LDO} > \text{Aut}\cdot\left(N\cdot E_{CYCLE}\right) \tag{7}$$

Based on an industrial requirement for temperature measurement a sampling rate of T_{CYCLE} = 5 min has been selected and the intended system location leads to Aut = 15 days of operating time without recharging. We choose V_{SC_MAX} = 5.3 V and V_{SC_MIN} = 3.3 V; assuming η_{LDO} = 75%, we obtain C_{EQ} = 12.5 F. Two supercapacitors with a value of C = 25 F each should be suitable. We have therefore chosen these values for the supercapacitors used.

Following our specifications, we choose a Nesscap model ESHSR-0025C0-002R7 as their main characteristics are: 25 F, 2.7 V, ESR 21 mΩ, [−40˚C, 65˚C], 500,000 cycles, 1000 hours at 85˚C.

For this project, we choose to store the energy at a maximum voltage of 5.2 V. This requires two supercapacitors in series. The maximum load level remains below the acceptable level of 5.4 V for the supercapacitors and 5.3 V for the SPV1050. This gives a safe range for the whole system.

If C_{EQ} corresponds to the equivalent capacity of two serial supercapacitors, energy of the pack E_{CAP} is given by:

$$E_{CAP} = \frac{1}{2}C_{EQ}\cdot V_{SC}^2 \tag{8}$$

2.4.2. Supercapacitors Self-Discharge

Supercapacitors self-discharge is a critical issue for systems in both following cases:

- They must remain fully charged a long period of time before being used,
- They are used as power sources with a low potential recharge level.

Self-discharge has been assessed using a preload of the two supercapacitors pack, previously placed in a thermostatic enclosure at constant voltage for 12 hours. The open circuit voltage evolution has been monitored, using a dedicated device (Biologic BCS810) as a voltmeter. The results are given in **Figure 5**.

Based on these measurements, the relative energy losses can be evaluated after 5 days as 1% of the initial energy at 5˚C, 3% at 25˚C and 12% at 45˚C.

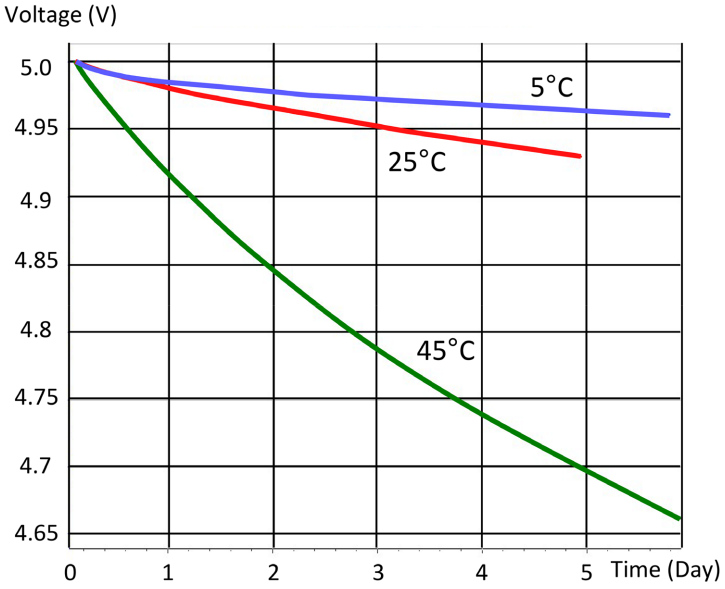

Figure 5. Influence of the temperature on self-discharge.

Losses increase with temperature but remains acceptable over a wide temperature range (3% @ 45˚C at the end of the first day).

The self-discharge current can be estimated from the slope of the curve using the following relationship:

$$I_{\text{SELFDISCH}} = C_{\text{EQ}} \cdot \frac{\Delta V_{\text{SC}}}{\Delta t} \tag{9}$$

For $\Delta t = 1$ day (from $t = 0$ to $t = 1$), a self-discharge current $I_{\text{SELFDISCH}} = 3$ µA @ 25˚C and 11 µA @ 45˚C has been measured. But some of this current is probably due to the charging of the slow branches of the supercapacitors.

For $\Delta t = 2$ days (from $t = 3$ to $t = 5$), we find $I_{\text{SELFDISCH}} = 2$ µA @ 25˚C and 6 µA @ 45˚C.

2.4.3. Balancing Circuit

One problem associated with the use of two supercapacitors connected in series is that the voltage across each capacitor cell can be different if the C values are different.

Cells manufacturers regard over-voltage as a form of misuse, leading to loss of capacitance, an increase in equivalent series resistance (ESR,) bulging, possible venting, electrolyte decomposition, gas generation, and ultimately reduced life.

A simple way to balance a string of supercaps is with paralleled resistors. A rule of thumb is the same factor-of-ten that can be used to make an unloaded voltage divider. Whatever the leakage current of the supercap, a parallel resistor that has ten times the current at the nominal cell voltage can be used.

This approach has several problems:

- It doesn't solve the tolerance imbalance problem,
- It adds resistor tolerances to the capacitor tolerance problem,
- The resistors will draw current that must be supply or it will discharge the

capacitor string,

- They also won't allow for variations in supercap leakage over time and temperature.

A much better solution is to use FET Transistors that will turn on slightly as the capacitor cell approaches the operating rated voltage. The FET manufacturer can control the threshold voltage with ion implantation of a floating gate, or by process, or by hand-selection: a more predictable and precise current at the cell voltage can be therefore considered.

Active balancing with FETs circuits is a more direct solution. The FETs will regulate the cell voltage and even considering for ageing and temperature changes.

In our application, we chose an ALD9100xx (xx denoting the nominal voltage), with xx = 24:2.4 V. This circuit (Figure 6) includes two MOSFETs, and the drain current increases with the voltage at the terminals of the MOSFET, which acts as a variable resistor. The variation is therefore, exponential, which allows a very small current to be consumed below the voltage used, 2.4 V. Above this, it favors the discharge of the supercapacitor.

Figure 7 describes the evolution of the current dissipated by the ALD910024 chip as a function of the voltage across the terminals of a supercapacitor. The total voltage in the study is limited to 5.2 V, *i.e.*, 2.6 V per supercapacitor.

In normal operation, the leakage current due to balancing remains less than 1 μA. If there were a voltage imbalance between the two supercapacitors in series, one reaching its maximum voltage of 2.7 V, then it would result in a leakage current of 240 μA. On the contrary, the other supercapacitor, which remains below 2.5 V, has a leakage current below 10 μA. It tends to balance the two voltages.

2.5. Energy Management

2.5.1. SPV1050 Circuit (Extract from Datasheet)

Various commercial ICs recover the energy from solar cells and manage both the MPPT function and the charge of the storage element (rechargeable battery or supercapacitor). For our application, we choose an SVP1050 from STM

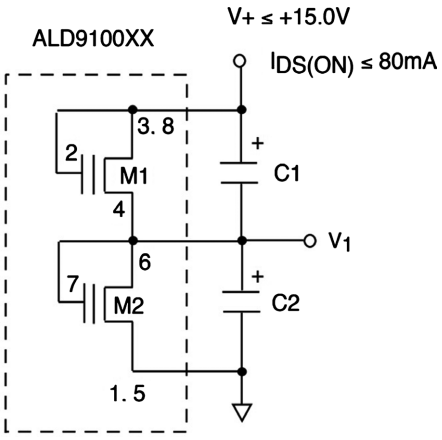

Figure 6. Internal scheme of the ALD9100xx circuit.

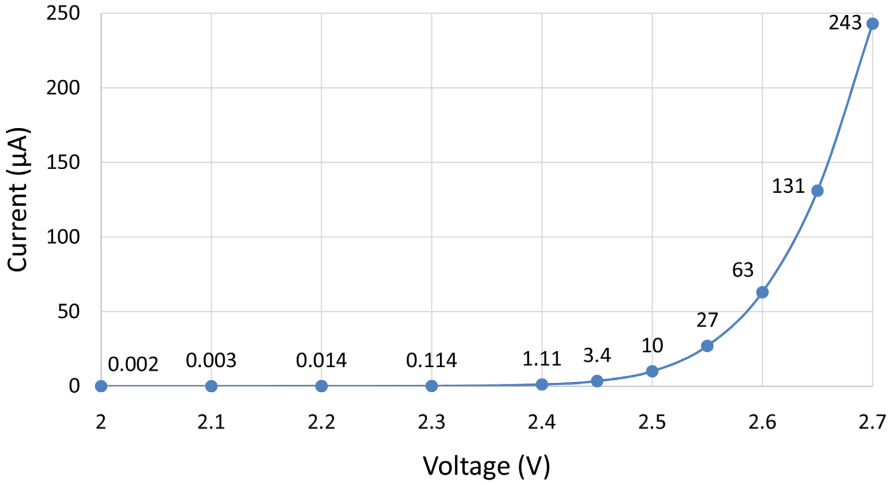

Figure 7. Measurements of the current dissipated by the ALD910024 chip vs the voltage at the terminals of a supercapacitor.

because it has the following features

- Maximum solar power extraction with MPPT control law with fraction of V_{OC} algorithm (the ratio is fixed using adjustable resistances),
- Charge management of the storage element (battery or supercapacitor) with adjustable end of charge and discharge voltage thresholds,
- Two independent LDO (1.8 V, 3.3 V, Imax 200 mA), each controllable via an Enable control pin.

Main features of this circuit are:

- Very wide solar voltage range: from 75 mV to 18 V, with a minimum voltage of 2.6 V and a minimum current of 5 µA for startup in Buck/Boost mode,
- For the storage stage, a load current ≤ 70 mA and a voltage between 2.2 V and 5.3 V,
- Consumption (datasheet):
  - Shutdown current before first startup or discharged battery ($V_{SC} < V_{UV}$) ~1 nA;
  - Standby current (inactive LDO_EN) ~1 µA;
  - Normal current without charge ~2 µA with 1LDO on ~3 µA with both LDO ON.

The different phases of operation (ON/OFF position of the PASS Transistor, Activation/Deactivation of the buck/boost and of the output LDO) are depending on the V_{STORE} voltage. Different configurations explained below are summarized on **Figure 8**.

2.5.2. PASS Transistor

In the SPV1050, an internal transistor named PASS (**Figure 9**) acts as a static switch. It allows the V_{STORE} potential to be disconnected from the V_{SC} potential of the storage stage (supercapacitors or batteries) if the storage voltage is too low. In this case, the consumption of the storage stage is minimized but the load isn't supplied.

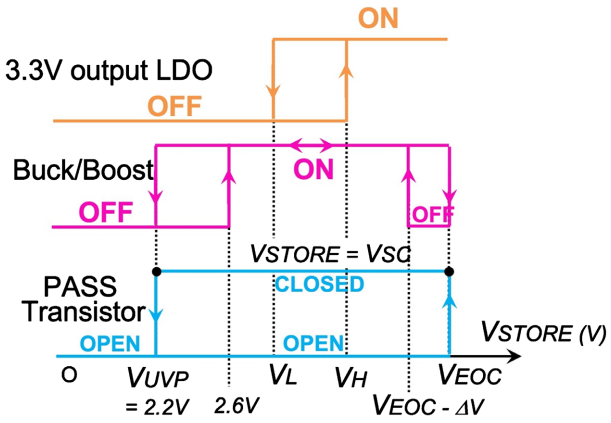

Figure 8. Summary of V_{STORE} (and V_{SC}) threshold voltages.

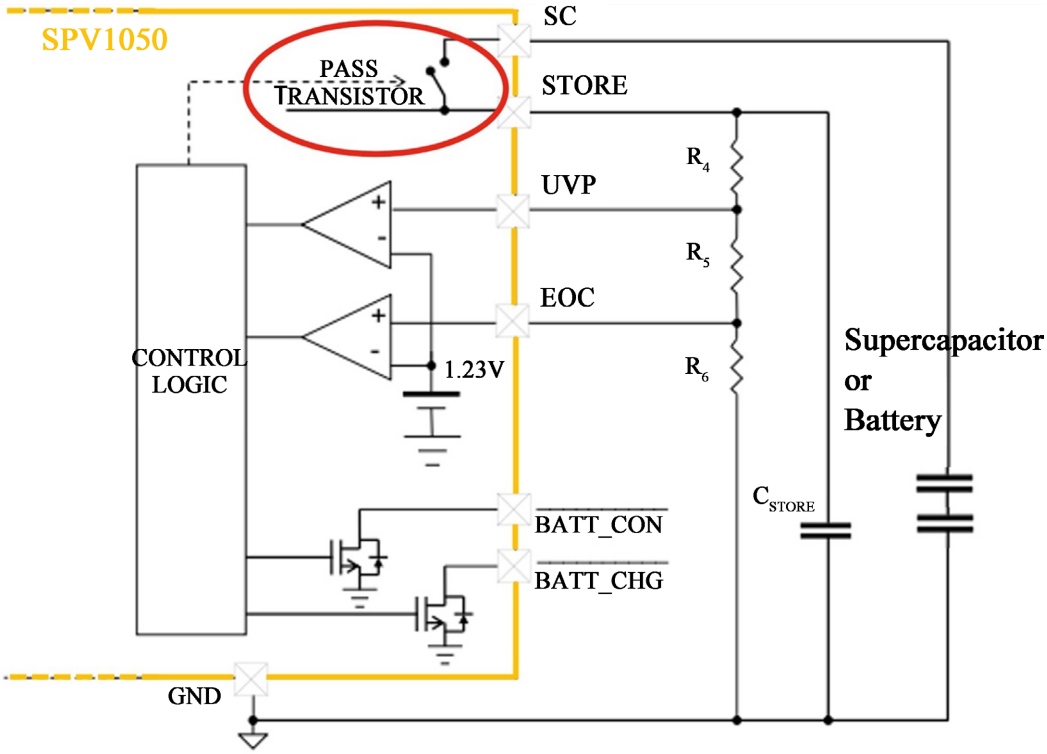

Figure 9. Charge stage threshold management (battery or supercapacitor), figure adapted from the technical documentation.

PASS is open prior to the first power-up. It closes when the V_{STORE} voltage rises to the V_{EOC} threshold and remains closed unless V_{STORE} falls below the V_{UVP} threshold.

The V_{UVP} and V_{EOC} thresholds are adjustable by a resistance set (R_4, R_5, R_6), according to the relationships given by the manufacturer. For our application, V_{UVP} = 2.2 V and V_{EOC} = 5.2 V.

2.5.3. Buck/Boost Converter and Working Phases

A DC/DC converter (Boost or Buck/Boost) is located between the solar panel and the storage stage. We chose the Buck/Boost configuration, due to PV Solar

input voltage variations.

1) Starting Mode Operation

At the initial startup, the converter doesn't switch. Instead, the positive pin of the photovoltaic source and the STORE pin are internally short-circuited. This phase lasts as long as $V_{STORE} < 2.6$ V.

When $V_{STORE} = 2.6$ V, the integrated Buck/Boost starts working properly. Once started, it will operate in MPPT Mode if $V_{UVP} \leq V_{STORE} < V_{EOC}$.

To fully understand the different phases during the startup, it is important to note that $C_{STORE} = 94$ µF is very small compared to $C_{EQ} = 12.5$ F. This means that it is necessary to charge and discharge many times C_{STORE} to fill C_{EQ}.

We assume that the system is initially empty, meaning $V_{STORE} = 0$ and $V_{SC} = 0$. The DC/DC is OFF. PASS is open. Initial startup starts as soon as the PV panel receives some light. V_{STORE} connected internally to V_{PV+} increases. The DC/DC starts switching as soon as V_{STORE} reaches 2.6 V. C_{STORE} fills and V_{STORE} reaches V_{EOC}. At this level, the PASS transistor closes, and in consequence, C_{STORE} discharges in C_{EQ}. Immediately, V_{STORE} falls under V_{UVP}, which means that PASS opens again, disconnecting C_{EQ} from C_{STORE}. As $V_{STORE} < V_{UVP}$, the converter also stops.

A new cycle begins but the circuit can't extract the maximum available power from the PV panel during this sequence. Gradually, the V_{SC} increases. Once V_{SC} reached V_{UVP}, PASS keeps closed and assuming that the harvested power is greater than the consumed power, V_{SC} continues to increase. When V_{SC} reaches 2.2 V, the DC/DC works continuously and the amount of harvested power increases as the DC/DC remains in MPPT mode. Figure 9 summarizes the process.

2) Nominal Mode Operation

After the initial startup, the PASS transistor is ON meaning $V_{STORE} = V_{SC}$.

It remains closed as long as $V_{STORE} > V_{UVP} = 2.2$ V.

If $V_{UVP} \leq V_{STORE} < V_{EOC}$, the converter works in maximum power point tracking (MPPT mode) with a « fraction of V_{OC} » algorithm. Due to circuit behavior, every 16 s, during 400 ms, the photovoltaic panel is placed in open circuit: the SPV1050 recovers the V_{OC} open circuit voltage. The DC/DC then works by regulating the PV panel voltage close to $V_{PV} = k.V_{OC}$. As exhibited in §3c, the V_{MPP} setpoint is located around 80% of the V_{OC} voltage. A set of two resistors fixes k = 0.8, which ensures that:

$$V_{PV} \approx V_{MPP} \approx k \cdot V_{OC} \tag{10}$$

When the V_{EOC} threshold is reached (*i.e.*, the storage stage is full), the DC-DC stops transferring power to avoid overloading. It starts again when $V_{STORE} < V_{EOC} - \Delta V$, with $\Delta V = 50$ mV.

3) Characterization

The DC/DC has been characterized (Figure 10) at different solar panel voltages and different V_{STORE} voltages. V_{STORE} is almost equal to V_{SC}, the difference being the voltage drop in the PASS transistor.

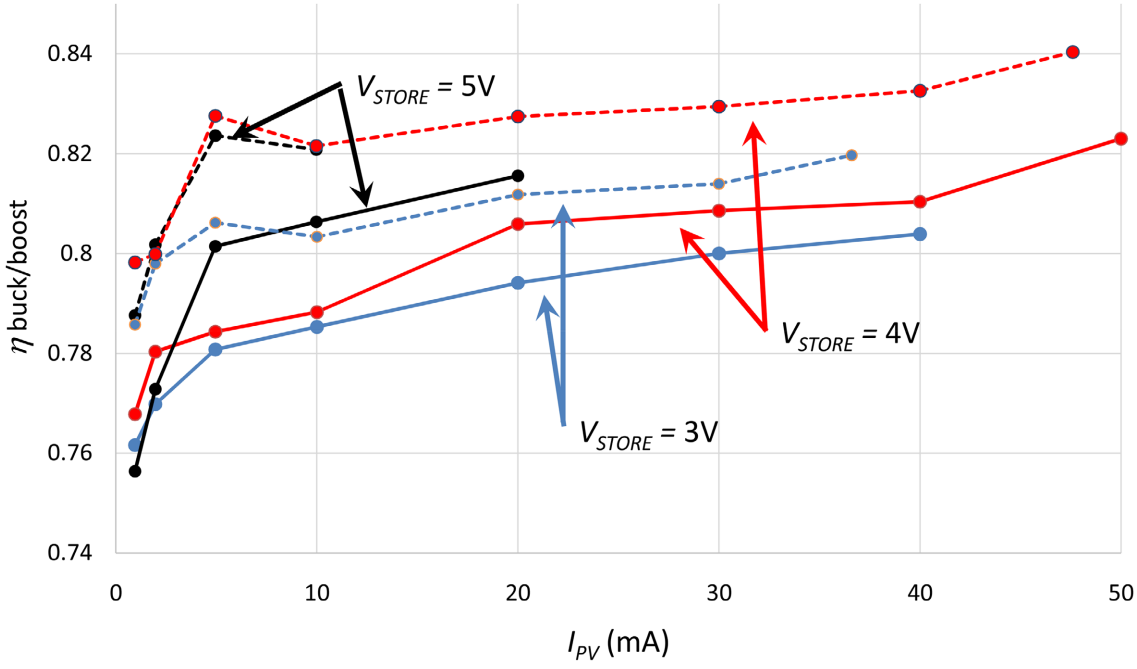

Figure 10. Buck/Boost efficiency @ V_{PV} = 3.4 V (continuous lines) and @ V_{PV} = 4.2 V (dotted lines).

For currents below 1 mA, the efficiency of the buck/boost converter is close to 70%. It is higher than 78% for currents > 2 mA, which is quite correct.

2.5.4. Output Stage

The SPV1050 incorporates an LDO to supply the output with the required voltage level (3.3V). The enable pin of the LDO is driven by an external hysteresis comparator, powered by the V_{STORE} voltage (**Figure 11**). The voltage measured by the comparator is the V_{SC} voltage.

1) Setting of the Comparator

During initial start-up, the load can draw a significant amount of energy from the supercapacitors, particularly in the case of an initial connection to a network. This leads to a voltage drop of the storage stage. At the end of startup, the storage level must always be above the minimum level accepted by the LDO for proper operation. It sets the minimum V_H level. For a large margin of safety, specially to assure a sufficient autonomy after start-up phase, V_H = 4.3 V has been chosen. V_L is set just below the nominal LDO output voltage at 3.2 V.

Resistors of the comparator are chosen in the way to set the V_H and V_L switching thresholds. The comparator resistors are selected in accordance with [39] to set the V_H and V_L thresholds.

2) LDO + PASS + Comp + Balancing Efficiency

The following measurements (**Figure 12**) show η_{LDO}, the ratio between the output power of the LDO and the output power of the supercapacitors (replaced by a voltage source for these measurements). In this situation, the solar panel is in the darkness, so there is no power from the PV panel. PASS is switched ON. The efficiency in this test includes losses of the LDO, the PASS transistor serial

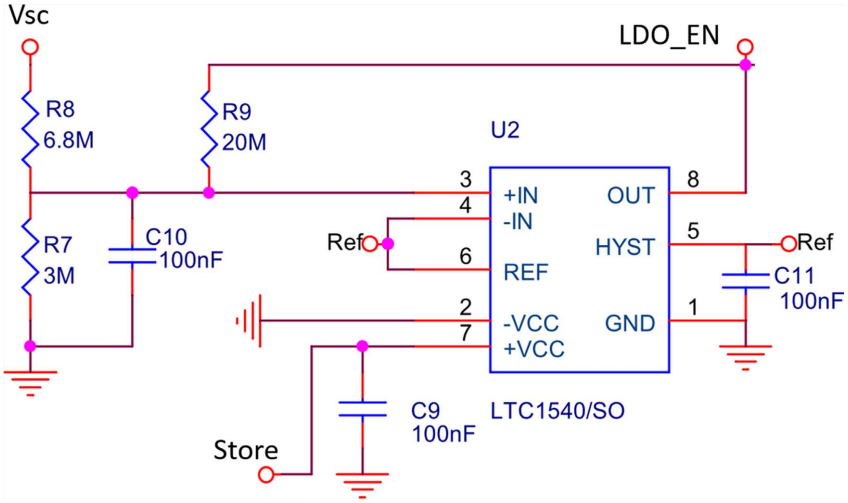

Figure 11. Hysteretic comparator.

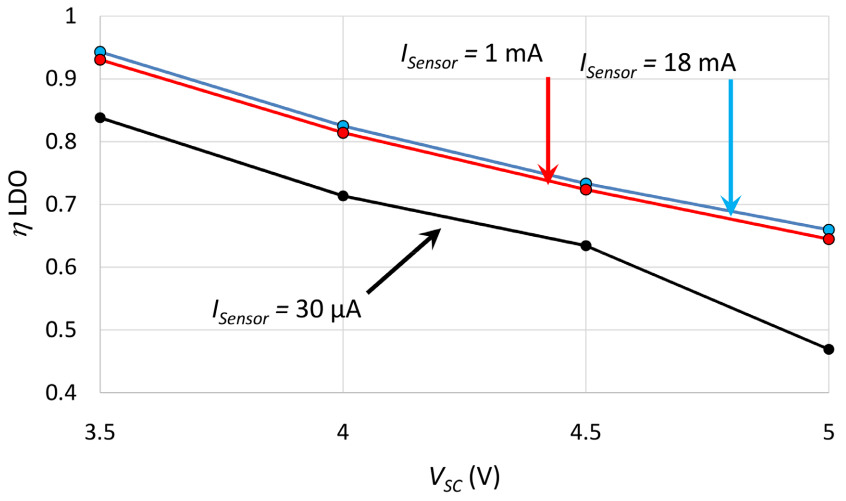

Figure 12. Output stage efficiency (LDO).

resistance (7 Ω), the comparator and the balancing circuit losses. Only self-discharge losses and Joule losses due to supercapacitor ESR are not included. Measurements were made to evaluate the performance of the system when the sensor node is in sleep mode and for the typical values during the active mode phase. Efficiency is independent of the current on the range 1 to 18 mA.

2.6. Full Circuit

Figure 13 shows the electrical diagram of the entire device, which is integrated on the board shown in Figure 14.

The overall size of the board is 40 × 47 mm^2. The board is placed in a box on which the solar panel is glued. The total price of the electronic components and the solar panel is around 20 € for a series of 1000 pieces. The choice of a CR2477 Lithium battery (3 V 1 Ah 5€) in similar conditions: T_{cycle} = 5 min, <P> = 58 µW gives an estimated autonomy of 5 years). The extra-cost of 15 € must be compared with the extra costs of the new coin and the cost of the technician to

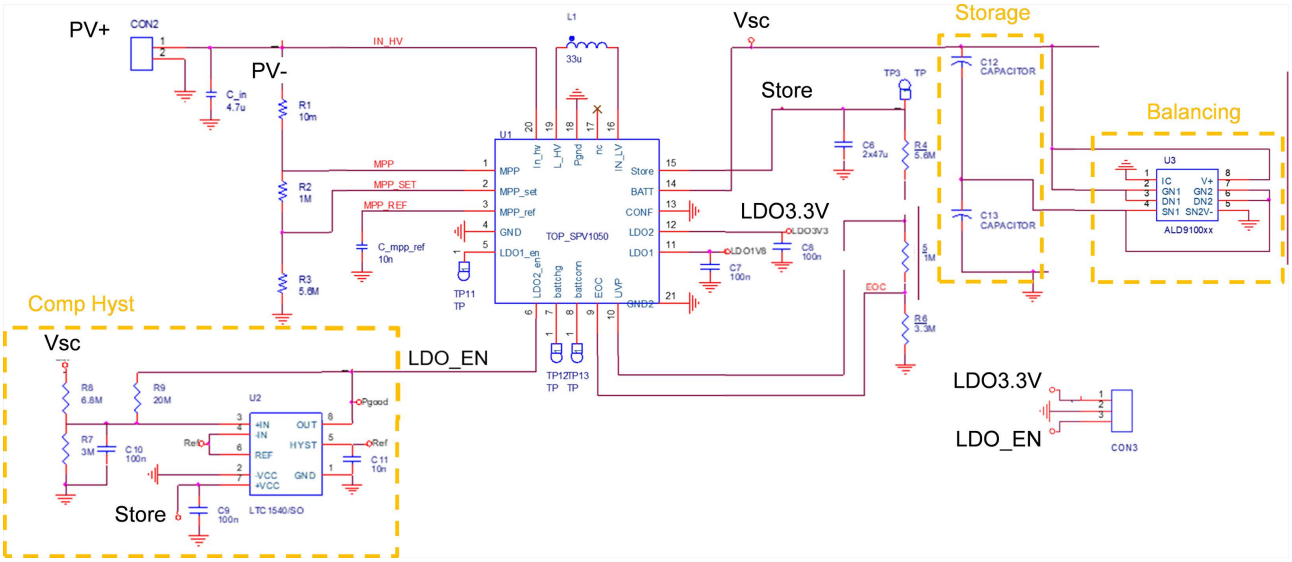

Figure 13. Electronic circuit.

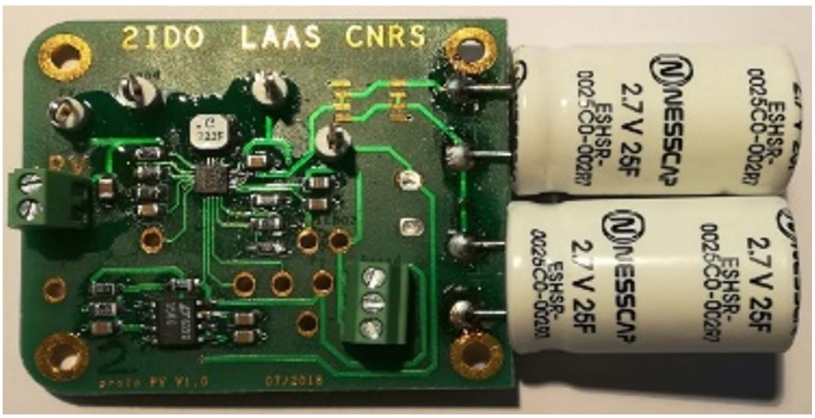

Figure 14. Electronic board.

replace the battery as with our battery-free system a work life of 10 years or more is expected.

3. The Issue of the Startup

3.1. First Initial Startup: Cold Start

Initially, the supercapacitors are empty, and the initial start-up begins as soon as the PV panel is illuminated. Figure 15 (obtained under constant light @ 6100 lux) summarizes the process. In this figure, the data is displayed and averaged every second. Once $< V_{STORE} >$ equal to $< V_{SC} >$ permanently, the buck-boost operates correctly but during the previous phase, the efficiency is very poor. In consequence, it is necessary to wait more than one day before powering the sensor.

This is unacceptable for most application. In fact, a response from the sensor is expected immediately after installation to check that everything is OK. So, even if supercapacitors storage solutions combined with energy harvesting look promising in terms of autonomy, temperature performance and price, this long

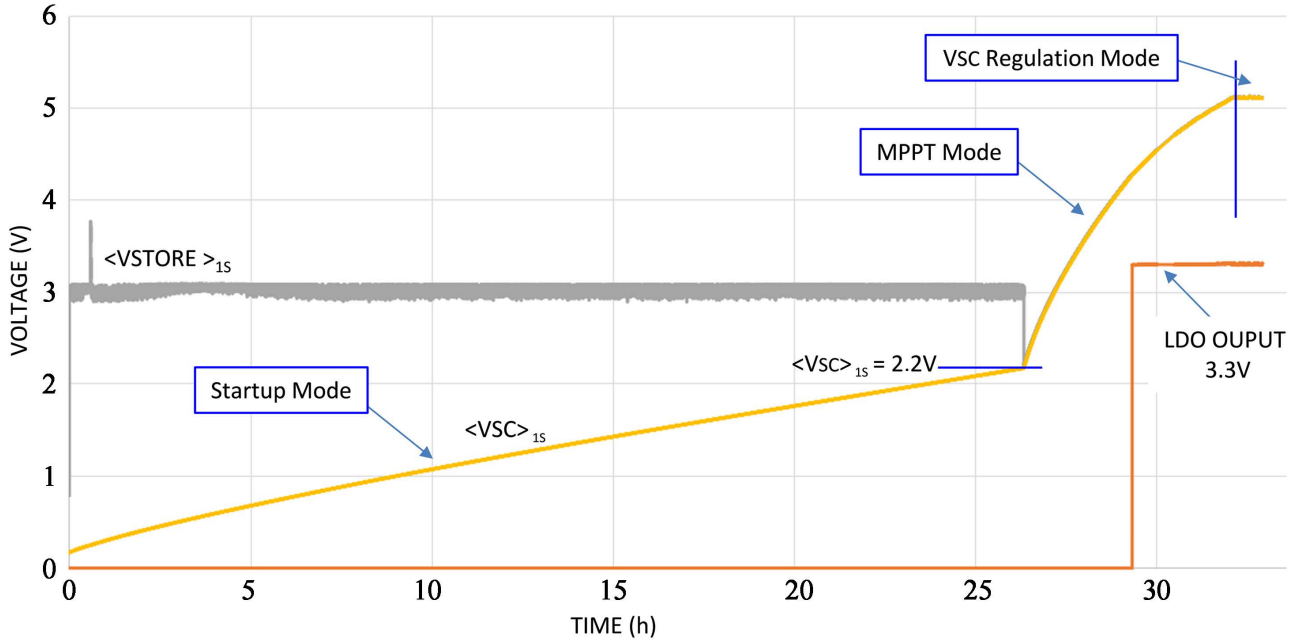

Figure 15. Cold start with supercapacitors initially discharged.

initial startup seems redhibitory for industrial applications.

Fortunately, as will be shown below, a judicious preload of the supercapacitors can avoid the problem of the duration of the first cold start and allow an immediate start. To our knowledge, this point has not been explained and developed in the literature.

Three conditions are required for immediate start:

1) precharging of the supercapacitors,

2) leak-free storage,

3) activation signal.

3.2. Preload Procedure

It is very important that the precharging process starts with the PASS transistor open to avoid unnecessary further consumption.

To guarantee this initial state, the solar panel must be placed in darkness. At the same time, the supercapacitors are discharged by means of an external dissipative resistor connected to their terminals until $V_{SC} < V_{UVP}$, which opens the PASS transistor. At this time, the device is not yet packaged or is packaged but with an external connector to allow access to the supercapacitors.

At this point the resistor is removed and PASS remains open. The supercapacitors are almost electrically isolated. In fact, they are always connected to the open PASS transistor, to the balancing circuit and there is still a wire to the hysteretic comparator.

The supercapacitors are then precharged to 5.2 V by connecting a voltage generator directly to their terminals. The generator is pre-set to 5.2 V and limited to 500 mA. When the precharge is complete, the generator is removed. The su-

percapacitors are then fully charged, but without powering the sensor node as PASS remains open.

As the precharge is carried out several hours or days before commissioning, the supercapacitors must remain sufficiently charged for a nominal boot. This requires the selection of supercapacitors with low self-discharge and a circuit design with low other consumptions (balancing, SPV1050 consumption before start-up, hysteretic comparator). These conditions are carried out, modelled and the experimental results are presented below.

3.3. Activation Signal

As explained previously, PV panel is covered with a black sheet and maintain in darkness. For an effective startup at the right time, it is simply necessary to illuminate the solar panel. The SPV1050 wakes up, V_{STORE} can go above V_{EOC}. Immediately PASS closes and the LDO is activated. This simple but effective solution has been validated with natural light and for a night start with the light (LED) of a mobile phone placed in front of the solar cells.

3.4. Consumption and Energy Autonomy after Preload

To evaluate the available lifetime before activation, it is necessary to estimate the global leakage current, sum of the equivalent self-discharge current ($I_{\text{SELFDISCH}}$) added with the balancing current (I_{BAL}) and the current absorbed by the SPV1050 and the comparator ($I_{\text{SPV+COMP}}$). Calculations show that the losses in the ESR of the supercapacitors are negligible. In this part, the PASS transistor is always open.

1) Currents Measurements and Modelization

In the paragraph §2.4.2, we note that $I_{\text{SELFDISCH}} < 2$ µA @ 25˚C. In our case, 2 µA is a reasonable value deduced from the linear shape of the self-discharge curve after a few days @ 25˚C. This value will be chosen for simulations.

When PASS is open, the cumulative $I_{\text{SPV+COMP}}$ consumption of both the SPV1050 circuit and the hysteresis comparator (COMP), is less than 0.5 µA. Measurements lead to the following modelling, with $I_{\text{SPV+COMP}}$ in A and V_{SC} in V.

$$I_{\text{SPV+COMP}} = 0.10 \cdot 1e^{-6} \cdot V_{\text{SC}} \tag{11}$$

I_{BAL} vs V_{SC} is deduced by multiplying the voltage by 2. It is determined as follow:

- Will be null if $V_{\text{SC}} < 4.6$ V,
- An order 1 model is suitable for V_{SC} between 4.6 V and 4.8 V. (overstatement in lost current),

$$I_{\text{BAL}} = \left(4.98 \cdot V_{SC} - 22.89\right) \cdot 1e^{-6} \tag{12}$$

- An order 3 model is ideal for VSC between 4.8 and 5.4 V with:

$$I_{\text{BAL}} = \left(1702.50 \cdot V_{SC}^3 - 24984 \cdot V_{SC}^2 + 122246 \cdot V_{SC} - 199431\right) \cdot 1e^{-6} \tag{13}$$

$I_{\text{SPV+COMP}}$ + I_{BAL} measurements with PASS is open, are obtained by replacing

the supercapacitors with a voltage source. The current supplied by the source is the sum of the balancing current added to the current consumed in the SPV1050 and in the comparator (Figure 16). In blue, the curve gives only the balancing current previously measured for a single supercapacitor (derived from Figure 8 by multiplying the voltage by 2). The measurements agree with our model.

Thereby, if 3.2 V < V_{SC} < 4.8 V, we note a global consumption close to 4 µA as $I_{SELFDISCH}$ ≈ 2 µA @ 25˚C, $I_{SPV+COMP}$ ≈ 0.5 µA and I_{BAL} < 1 µA.

It allows preloading long before commissioning.

2) Autonomy

Starting from $V_{SC}(0)$ = 5.2 V, with a pitch Δt of 1 h, the evolution of the V_{SC} voltage is calculated iteratively by discretizing the classical equation of a capacitor ($I_{SC} = C.\,\mathrm{d}V_{SC}/\mathrm{d}t$) using the following relationship and expressing $V_{SC}(n+1)$ according to $V_{SC}(n)$ and the other parameters. The influence of supercapacitors ESR is neglected as $V_{ESR} = 2 \cdot \mathrm{ESR} \cdot \left(I_{BAL} + I_{SPV+COMP}\right) < 2 \cdot 21 \cdot 3.4\mathrm{e}{-6} = 0.14$ mV.

$$\begin{aligned} & I_{SELFDISCH}(n) + I_{BAL}(n) + I_{SPV+COMP}(n) \\ & = C_{EQ} \cdot \frac{\Delta V_{SC}}{\Delta t} = C_{EQ} \cdot \frac{V_{SC}(n+1) - V_{SC}(n)}{\Delta t} \end{aligned} \tag{14}$$

The results of the simulation with $I_{SELFDISCH}$ = 2 µA are exhibited on Figure 17 and compared with the practical test. It shows as expected that the voltage (dashed curve with $I_{SELFDISCH}$ = 2 µA) drops rapidly as long as V_{SC} > 4.8 V. This is explained by the energy dissipation within the supercapacitors balancing. Self-discharge then becomes dominant.

Figure 17 shows the importance of the self-discharge current of the supercapacitors in the evaluation for the autonomy. The voltage drops faster than expected, this is largely due to the power consumption of the measuring system (voltmeter with too much input capacity). Anyway, with a preload of the supercapacitors more than 15 days before, the device remains operational for an immediate boot (as V_{SC} > V_H = 4.3 V).

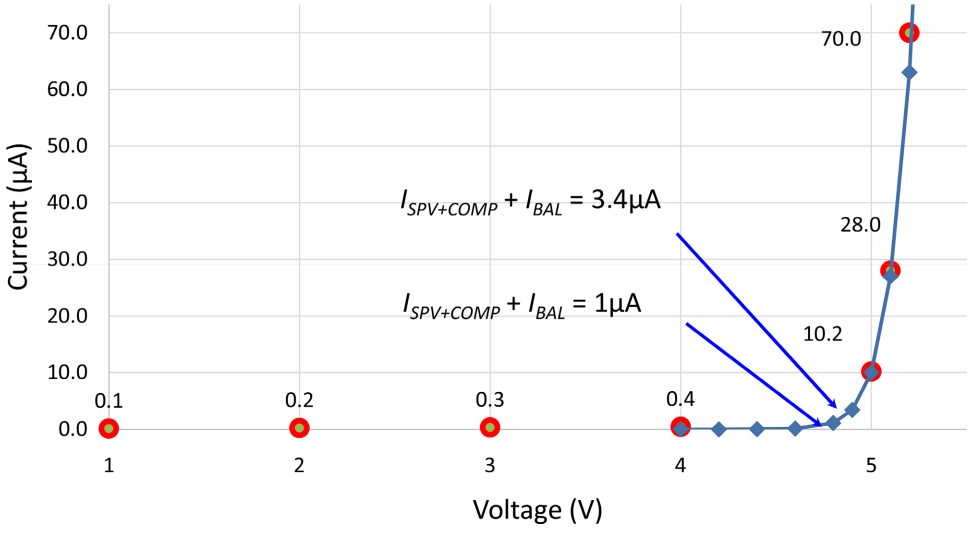

Figure 16. Sum of currents (balance, SPV1050 and comparator) when PASS is open.

4. Experimental Results and Discussion

4.1. Indoor Measurements

The sensor node is in a room (Figure 18). There is a window nearby but no direct light. The sensor measures the voltage of the supercapacitors, the ambient temperature, and the luminosity. It transmits that information on a microcomputer connected to the Internet using the Jeedom software. The device is set to a measurement cycle of 5 minutes.

Figure 19 shows the evolution of the measured values. We observe the daily cycle: energy harvesting during the day and recharging of the supercapacitors to a maximum level of 5.2 V, consumption without recharging at night and therefore discharge of the supercapacitors. The constant level of the voltage in the middle of Figure 20 shows that a light intensity of 200 lux is just enough to compensate the device's power consumption.

4.2. Autonomy after Activation

4.2.1. Modelisation

On the basis of the previous measurements, the autonomy is calculated iteratively

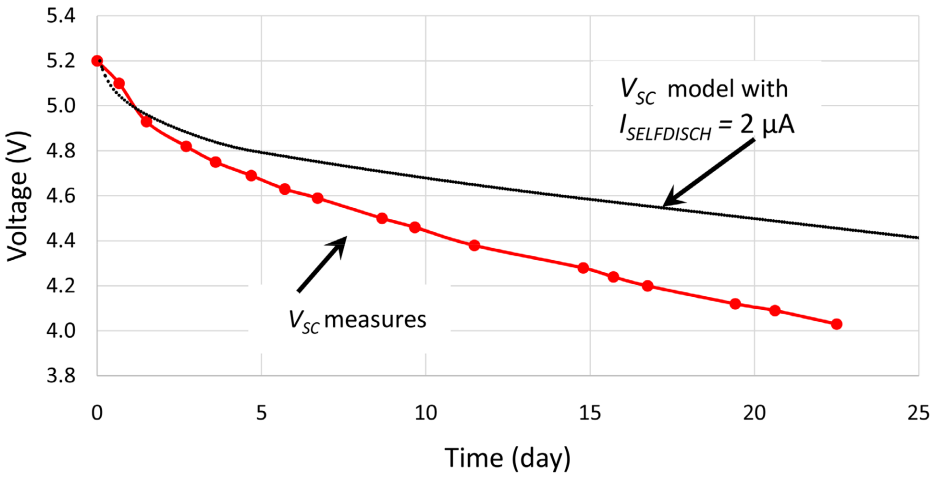

Figure 17. V_{SC} evolution (models and measures @T ≈ 20˚C), PASS open.

Figure 18. Photo of the device in a room, without direct lighting.

by performing the energy, noted $E'_{\mathrm{CYCLE}}(n)$, drawn during the nth cycle at the level of the supercapacitors. In this assessment, we must consider the active phase of the node, the standby phase, and the losses due to self-discharge, to supercapacitors ESR and to the internal resistance of the transistor PASS (R_{DSON} = 7 Ω).

$$E'_{\mathrm{CYCLE}}(n) = E'_{SLEEP} + E'_{\mathrm{MEAS}} + E_{\mathrm{SELFDISCH}} + E_{\mathrm{ESR}} + E_{\mathrm{PASS}} \tag{15}$$

with

$$E'_{\mathrm{SLEEP}} = E_{\mathrm{SLEEP}} / \eta_{\mathrm{LDO}}(I_{\mathrm{SLEEP}})$$

and

$$E'_{\mathrm{MEAS}} = E_{\mathrm{MEAS}} / \eta_{\mathrm{LDO}}(I_{\mathrm{MEAS}})$$

Figure 19 is used to modelise η_{LDO} as $V_{\mathrm{SC}} \in [3.3; 5.3]$ V, in the form of first orders:

$$\eta_{\mathrm{LDO}}(I_{\mathrm{SLEEP}} = 11\,\mu\mathrm{A}) = -0.237 \cdot V_{\mathrm{SC}} + 1.672 \tag{16}$$

$$\eta_{\mathrm{LDO}}(I_{\mathrm{MEAS}} = 18\,\mathrm{mA}) = -0.198 \cdot V_{\mathrm{SC}} + 1.629 \tag{17}$$

Self-discharge losses are estimated with a constant self-discharge current $I_{\mathrm{SELFDISCH}}$ = 2 µA, so:

$$E_{\mathrm{SELFDISCH}} = I_{\mathrm{SELFDISCH}} \cdot V_{\mathrm{SC}} \cdot T_{\mathrm{CYCLE}} \tag{18}$$

Losses due to serial resistors of supercapacitors and PASS are:

$$E_{\mathrm{ESR}} = 2 \cdot \mathrm{ESR} \cdot \left(I^2_{\mathrm{SLEEP}} \cdot (T_{\mathrm{CYCLE}} - T_{\mathrm{SLEEP}}) - I^2_{\mathrm{MEAS}} \cdot T_{\mathrm{MEAS}}\right) \tag{19}$$

$$E_{\mathrm{PASS}} = R_{\mathrm{DSON}} \cdot \left(I^2_{\mathrm{SLEEP}} \cdot (T_{\mathrm{CYCLE}} - T_{\mathrm{SLEEP}}) - I^2_{\mathrm{MEAS}} \cdot T_{\mathrm{MEAS}}\right) \tag{20}$$

These losses are negligible compared to other terms.

We calculate the energy lost $E'_{\mathrm{CYCLE}}(n)$ for each cycle and we deduce the new voltage of the supercapacitors after a T_{CYCLE} time. At the end of n measurement cycles, we have:

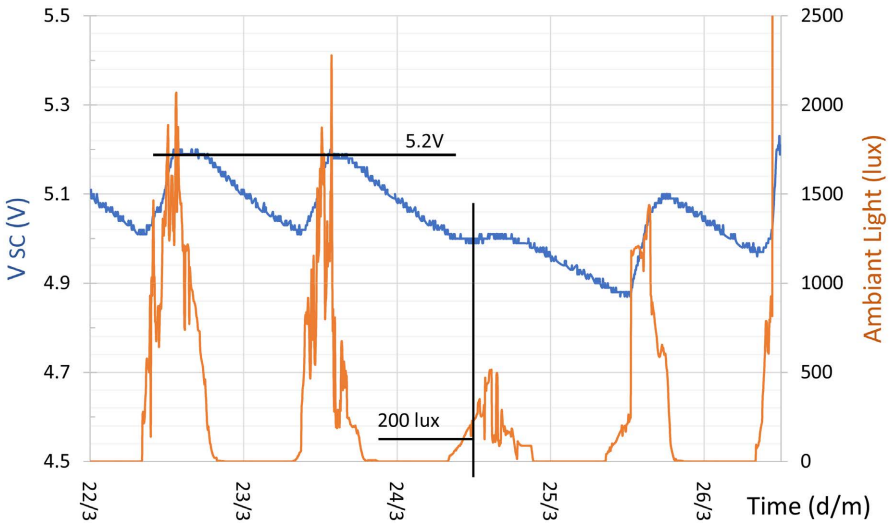

Figure 19. Evolution of the brightness and VSC over four days.

$$E_{CAP}(n+1) = E_{CAP}(n) - E'_{CYCLE}(n) \tag{21}$$

And reversing the equation

$$E_{CAP}(n+1) = \frac{1}{2} C_{EQ} \cdot V_{SC}^2(n+1) \tag{22}$$

We obtain V_{SC} for the next iteration.

With $I_{SELFDISCH}$ = 2 µA, we find 11.9 days of battery life respectively with a measurement rate of 5 minutes when the V_{SC} drops from 5.2 V to 3.4 V. This is in line with the 15 days required when sizing supercapacitors because when sizing supercapacitors, self-discharge was neglected and LDO efficiency was slightly overestimated.

4.2.2. Experimental Result

To evaluate the real operating life without any harvesting, the sensor node is placed in a black box. The evolution of the V_{SC} voltage is shown in Figure 20. The last data transmission is obtained at a voltage equal to 3.4 V. An autonomy of 11.8 days is measured. This confirms that the model is correctly validated with a self-discharge current of 2 µA as measured during the initial tests.

From the simulation results, we deduce, that with $I_{SELFDISCH}$ equal 2 µA, the energy repartition from supercapacitors is as follows:

- 61% powers the sensor node,
- 28% is lost for powering the electronic of the SPV1050, the LDO and the comparator,
- 9% is due to self-discharge of the supercapacitors and the PASS transistor is responsible of only 1% of the losses.

We notice that the global efficiency between the supercapacitors and the sensor node is close to 61%. The results show that the choice of supercapacitors with low leakage current is crucial to achieve a high level of autonomy.

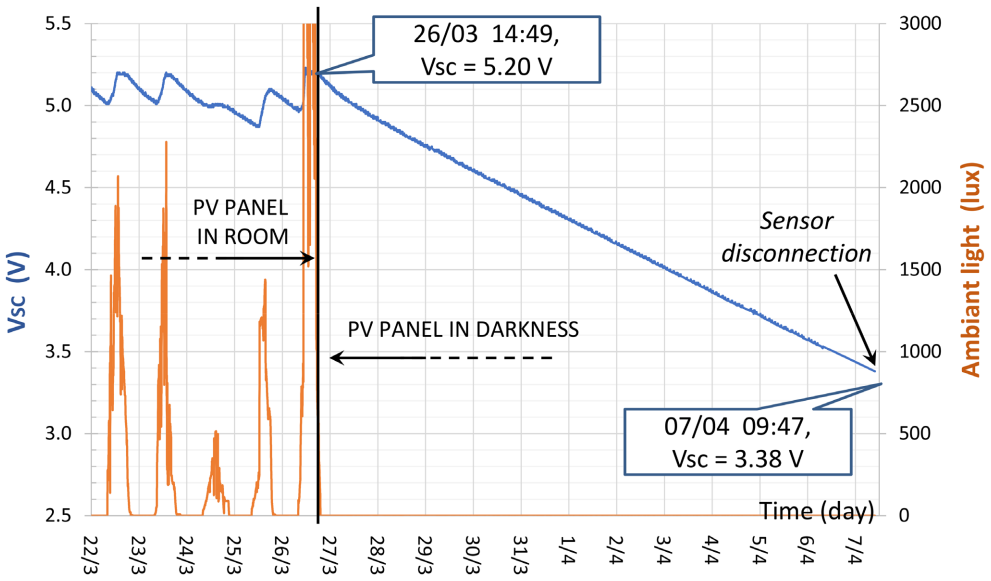

Figure 20. Operating life measurement.

5. Discussion

Various tests have been carried out over more than six months with indoor and outdoor sensor nodes. The results show that the system works perfectly in a range of indoor and outdoor lighting conditions and temperatures.

The original method presented to ensure the start at the right time is simple and works very well. However, it is necessary to discharge the supercapacitor below the V_{UVP} level (2.2 V) before precharging to ensure that the PASS transistor remains open.

If the output is 3.3 V or 1.8 V, it is easier to use the internal LDO of the SPV1050. If a different output voltage value is required, an external LDO or a DC/DC Buck must be added. To drain the supercapacitors almost completely, it can be interesting to use an external DC/DC Buck/Boost or an elevator followed by an LDO instead. Similarly, an external LDO or DC/DC connected directly to the supercapacitors is suitable to avoid losses from the PASS transistor which has a high resistance (7 Ω).

The SPV1050 is an easy-to-use circuit, but the photovoltaic current is limited to 70 mA. Consequently, if the panel surface is too large or on sunny day, the internal DC/DC will no longer operate in MPPT mode but in current limiting mode, which involves less power. The limitation is interesting for safety reasons as a system designed for indoor use in low light conditions will not suffer when exposed in full sunlight.

6. Conclusions

This paper presents the design, modelling, and characterization of an autonomous DC power supply (3.3 V, 200 mA, autonomy 11 days in darkness). Without a battery, using photovoltaic energy harvesting, the device is devoted to powering a wireless sensor node (3.3 V, Ipeak 18 mA, $<P> = 58$ µW).

Simple, and inexpensive, this system is modular for various light levels (indoor and outdoor). It is easy to integrate into a sensor node and use only off-the-shelf circuits. The size of the photovoltaic surface (35 cm^2) and the value of the supercapacitors (2x 25F, 2.5 V) have been explained for continuous operation, considering the solar potential and the consumption.

Once correctly preloaded and installed, the device can start at the desired time (within 15 days) using any light source as a trigger, such as the LED of a mobile phone. The paper highlights this interesting functionality, which to our knowledge has never been explained in the literature. The same procedure could be reused on another circuit such as the BQ25504.

We have thus shown that this device provides a permanent power supply with a minimum brightness (200 lux), for an acceptable extra cost (€15), compared with a solution with a battery but without future maintenance and replacement.

Acknowledgements

This work was carried out as part of the 2IDO project (Internet Industriel Des

Objets et Des Opérateurs) financed by the BPI (Banque Publique d'Investissement) as part of a PIA (Programme d'Investissements d'Avenir).

Conflicts of Interest

The authors declare no conflicts of interest regarding the publication of this paper.

References

[1] Kamienski, C., Soininen, J.P., *et al.* (2019) Smart Water Management Platform: IoT-Based Precision Irrigation for Agriculture. *Sensors*, **19**, Article 276. https://doi.org/10.3390/s19020276

[2] Wu, F., Wu, T. and Yuce, M.R. (2019) An Internet-of-Things (IoT) Network System for Connected Safety and Health Monitoring Applications. *Sensors*, **19**, Article 21. https://doi.org/10.3390/s19010021

[3] Klaina, H., *et al.* (2022) Analysis of Low Power Wide Area Network Wireless Technologies in Smart Agriculture for Large-Scale Farm Monitoring and Tractor Communications. *Measurement*, **187**, Article ID: 110231. https://doi.org/10.1016/j.measurement.2021.110231

[4] Move Solutions Product. https://www.movesolutions.it/wp-content/uploads/Tiltmeter-Datasheet-Move-Solutions.pdf

[5] BT610 Battery Estimation Calculator | Laird Connectivity. https://www.lairdconnect.com/iot-devices/bluetooth-iot-devices/sentrius-bt610-io-sensor

[6] Battery Life Calculator. https://www.elsys.se/en/battery-life-calculator/

[7] Milesight IoT Product. https://www.milesight-iot.com/lorawan/sensor/em300-th

[8] Wika IoT Products. https://iiot.wika.com/

[9] DCO Systems Products. https://dcosystems.co.uk/wireless-industry-sensors/

[10] Kaushal, A. and Prakash, S. (2019) Solar Energy Harvesting in Wireless Sensor Networks: A Survey. 2019 6*th International Conference on Computing for Sustainable Global Development* (*INDIACom*), New Delhi, 13-15 March 2019, 224-229.

[11] Sidibe, A., Loubet, G., Takacs, A. and Dragomirescu, D. (2022) A Multifunctional Battery-Free Bluetooth Low Energy Wireless Sensor Node Remotely Powered by Electromagnetic Wireless Power Transfer in Far-Field. *Sensors*, **22**, Article 4054. https://doi.org/10.3390/s22114054

[12] Mabon, M., Gautier, M., *et al.* (2019) The Smaller the Better: Designing Solar Energy Harvesting Sensor Nodes for Long-Range Monitoring. *Wireless Communications and Mobile Computing*, **2019**, Article ID: 2878545. https://doi.org/10.1155/2019/2878545

[13] Tsiropoulos, Z. and Gravalos, I. (2022) A Comparative Analysis between Battery- and Solar-Powered Wireless Sensors for Soil Water Monitoring. *Applied Sciences*, **12**, Article 1130. https://doi.org/10.3390/app12031130

[14] Yue, X., Kauer, M., *et al.* (2017) Development of an Indoor Photovoltaic Energy Harvesting Module for Autonomous Sensors in Building Air Quality Applications. *IEEE Internet of Things Journal*, **4**, 2092-2103. https://doi.org/10.1109/JIOT.2017.2754981

[15] Petrariu, A.I., Lavric, A., Coca, E. and Popa, V. (2021) Hybrid Power Management

System for LoRa Communication Using Renewable Energy. *IEEE Internet of Things Journal*, **8**, 8423-8436. https://doi.org/10.1109/JIOT.2020.3046324

[16] Abella, C.S., *et al.* (2019) Autonomous Energy-Efficient Wireless Sensor Network Platform for Home/Office Automation. *IEEE Sensors Journal*, **19**, 3501-3512. https://doi.org/10.1109/JSEN.2019.2892604

[17] Opus Product. https://myopus.eu/en/products/smarthome/monitor/5/opus-water-detector-instant-detector

[18] Kasama, T., Koide, T., *et al.* (2019) Low Cost and Robust Field-Deployable Environmental Sensor for Smart Agriculture. 2*nd International Symposium on Devices, Circuits and Systems* (*ISDCS*), Higashi-Hiroshima, 6-8 March 2019, 1-4. https://doi.org/10.1109/ISDCS.2019.8719262

[19] Enocean Product. https://perpetuum.enocean.com/01-2022-en/vibration-sensor-for-monitoring-operation-and-failure-of-plants/?lang=en

[20] Elsys Product. https://www.elsys.se/shop/product/ers-eco/?v=f003c44deab6

[21] Turos, L.-Z., Csernáth, G. and Csenteri, B. (2018) Power Management in IoT Weather Station. 2018 *International Conference and Exposition on Electrical and Power Engineering* (*EPE*), Iasi, 18-19 October 2018, 133-138. https://doi.org/10.1109/ICEPE.2018.8559865

[22] Maita, F. and Maiolo, L. (2021) Low Power Wireless Sensor Network for Precision Agriculture: A Battery-Less Operation Scenario. 2021 *IEEE International Workshop on Metrology for Agriculture and Forestry* (*MetroAgriFor*), Trento-Bolzano, 3-5 November 2021, 75-79. https://doi.org/10.1109/MetroAgriFor52389.2021.9628772

[23] Yue, X., Kiely, J., Gibson, D. and Drakakis, E.M. (2020) Charge-Based Supercapacitor Storage Estimation for Indoor Sub-mW Photovoltaic Energy Harvesting Powered Wireless Sensor Nodes. *IEEE Transactions on Industrial Electronics*, **67**, 2411-2421. https://doi.org/10.1109/TIE.2019.2896321

[24] Šolić, P., Leoni, A., Colella, R., Perković, T., Catarinucci, L. and Stornelli, V. (2021) IoT-Ready Energy-Autonomous Parking Sensor Device. *IEEE Internet of Things Journal*, **8**, 4830-4840. https://doi.org/10.1109/JIOT.2020.3031088

[25] Gyanchandani, V., Masabi, S.N. and Fu, H. (2021) A Self-Powered Wearable Device Using the Photovoltaic Effect for Human Heath Monitoring. 2021 *IEEE* 20*th International Conference on Micro and Nanotechnology for Power Generation and Energy Conversion Applications* (*PowerMEMS*), Exeter, 6-8 December 2021, 60-63. https://doi.org/10.1109/PowerMEMS54003.2021.9658359

[26] Mathis, S., Gruber, J.-M., Ebi, C., Bloem, S., Rieckermann, J. and Blumensaat, F. (2022) Energy Self-Sufficient Systems for Monitoring Sewer Networks. 21*th ITG/GMA-Symposium on Sensors and Measuring Systems*, Nuremberg, 10-11 May 2022, 1-8.

[27] Elizalde, J., Cruces, C., Sandoval, M.S., Eguiluz, X. and Val, I. (2021) Self-Powered Photovoltaic Bluetooth® Low Energy Temperature Sensor Node. *IEEE Access*, **9**, 111305-111314. https://doi.org/10.1109/ACCESS.2021.3103388

[28] Meli, M., *et al.* (2020) Low Light Energy Autonomous LoRaWAN Node. 2020 *IEEE* 5*th International Symposium on Smart and Wireless Systems within the Conferences on Intelligent Data Acquisition and Advanced Computing Systems* (*IDAACS-SWS*), Dortmund, 17-18 September 2020, 1-6. https://doi.org/10.1109/IDAACS-SWS50031.2020.9297089

[29] https://devzone.nordicsemi.com/nordic/nordic-blog/b/blog/posts/intro-to-shockbu

rstenhanced-shockburst

[30] https://www.mysensors.org/

[31] https://www.jeedom.com/site/fr/

[32] https://power.larc.nasa.gov/data-access-viewer/

[33] https://re.jrc.ec.europa.eu/pvg_tools/en/

[34] Randall, J.F. and Jacot, J. (2002) The Performance and Modelling of 8 Photovoltaic Materials under Variable Light Intensity and Spectra. LPM, IPR, STI, EPFL, CH-1015 Lausanne, Switzerland.

[35] Matiko, J.W., Grabham, N.J., *et al.* (2014) Review of the Application of Energy Harvesting in Buildings. *Measurement Science and Technology*, **25**, Article ID: 012002. https://doi.org/10.1088/0957-0233/25/1/012002

[36] Waltisperger, G. (2011) Architectures intégrées de gestion de l'énergie pour les microsystèmes autonomes. Ph.D. Dissertation, Université de Grenoble, France. https://theses.hal.science/tel-00601784/

[37] Huet, F. and Boitier, V. (2019) Design Strategy of Conventional Electronic for Wireless Sensor Node Powered by Vibration Energy Harvester. *International Conference on Renewable Energies and Power Quality*, Tenerife, 10-12 April 2019, 555-560. https://doi.org/10.24084/repqj17.375

[38] Ibrahim, T., Stroe, D., *et al.* (2021) An Overview of Supercapacitors for Integrated PV—Energy Storage Panels. 2021 *IEEE* 19*th International Power Electronics and Motion Control Conference* (*PEMC*), Gliwice, 25-29 April 2021, 828-835. https://doi.org/10.1109/PEMC48073.2021.9432540

[39] Dutta, A., Mitra, S., *et al.* (2023) A Comprehensive Review on Batteries and Supercapacitors: Development and Challenges Since Their Inception. *Energy Storage*, **5**, e339. https://doi.org/10.1002/est2.339